

Coupled Multi-Electrode Investigation of Crevice Corrosion of AISI 316 Stainless Steel

Florent Bocher, Francisco Presuel-Moreno, Noah D. Budiansky, John R. Scully
116 Engineer's Way
University of Virginia
P.O. Box 400745
Charlottesville, VA
22904-4745
U.S.A.

Abstract

Close packed coupled multi-electrodes arrays (MEA) simulating a planar electrode were used to measure the current evolution as a function of position during initiation and propagation of crevice corrosion of AISI 316 stainless steel. Scaling laws derived from polarization data enabled the use of rescaled crevices providing spatial resolution. Crevice corrosion of AISI 316 stainless steel in 0.6 M NaCl at 50°C was found to initiate close to the crevice mouth and to spread inwards with time. The local crevice current density increased dramatically over a short period to reach a limiting value.

Introduction

Crevice corrosion is currently studied using either one of two conventional techniques depending on the information required. The first method involves two multi-crevice formers or washers fastened on both sides of a sample sheet. This technique provides exposure information on the severity of crevice corrosion (depth, position and frequency of attack) but delivers little or no electrochemical information.¹ The second method involves the potentiodynamic or potentiostatic

study of an uncreviced sample in a model crevice solution or under a crevice former in aggressive solution where crevice corrosion may initiate and propagate.² However, crevice corrosion initiation and propagation behavior is highly dependent on time and exact location in the crevice. The distance from the crevice mouth will affect the solution composition, the pH, the ohmic drop and the true potential in the crevice. These, in turn, affect the electrochemical factors controlling the reaction rate as a function of potential and position. This feedback process ultimately controls the morphology and depth of attack but most of these details are difficult to investigate.

Multi-electrode array can provide combined spatial and temporal resolution of electrochemical properties within the crevice. A Multi-Channel Micro-Electrode Analyzer^a (MMA) has recently been used to demonstrate the interaction between localized corrosion sites (pitting corrosion and intergranular corrosion).^{3 4} Coupled MEAs can provide combined spatial and temporal resolution of electrochemical properties of metallic surfaces. Individually electrically isolated electrode elements are coupled together, through in-line zero resistance ammeters, to form a galvanically coupled electrode surface designed to closely simulate a planar electrode surface but allow current behavior of each electrode to be monitored. Coupled MEAs have been successfully used in the investigation of many different corrosion phenomena: The interactions between localized corrosion sites (pitting corrosion and intergranular corrosion)^{3, 4}, the lateral propagation of general corrosion on carbon steel in concrete environments⁴, and the investigation of persistent vs. switching anodes and cathodes on Cu in drinking water systems.⁴ Additionally, MEAs constructed from Al alloys and the combination of Al alloys and Cu have been used to

^a Trade name from Scribner Associates, Inc.

investigate second-phase particle influences on localized corrosion ⁵ and the affect of chromate conversion coatings on anode and cathode behavior.⁶

By coupling such a tool with scaling laws derived from experimental data (a simple equation linking crevice depth/gap combinations having equivalent electrochemical conditions), it is possible to produce highly instrumented crevices, rescaled to enable spatial resolution of the local electrochemistry of corrosion processes.

Crevice corrosion is highly dependent on spatial and temporal details as expected based on different crevice corrosion stabilization models. According to Ohmic models for crevice corrosion, the potential at some position in the crevice must drop below the Flade potential E_{Flade} to stabilize crevice corrosion.⁷ According to chemistry change models, the solution concentration and pH must exceed critical values associated with depassivation of the initially passive alloy.⁸

In the case of stainless steel, it has been proposed that the MnS inclusions dissolve producing thiosulfate and sulfur ⁹, or sulfide.¹⁰ When a critical concentration is reached, crevice corrosion was predicted to initiate near inclusions.⁹ It has also been suggested that crevice corrosion initiates at the sites of metastable pitting corrosion.^{11 12}

The crevice depth and gap affect the solution composition, the pH, the ohmic potential drop and the true potential in the crevice.¹³⁻¹⁶ These in turn affect the current density as a function of external potential and position during the initiation, stabilization and repassivation stages. Crevices must be rescaled in order to increase spatial resolution to utilize coupled multi-electrode arrays to shed light on these processes. Moreover, rescaled systems (with individual electrode on the scale of tens or hundreds of micrometers) can more easily incorporate commercially available and technologically relevant alloys (often available as wire, sheet, or

film) allowing industrially meaningful experiments. This letter presents initial results on crevice initiation and propagation.

Experiments

The coupled MEA used conjointly with the MMA was composed of one hundred wires in a five by twenty formation inserted in a groove of a rod of the same metal as the wires. The diameter of the wires (250 μm) was chosen so that x_{crit} (critical initiation distance from the crevice mouth) and the expected zone of crevice corrosion (predicted from the scaling law) would be larger than the radius of a single wire. Figure 1(a) illustrates an array encased in a stainless steel rod. Such a system simulates a flush mounted planar electrode, with the 100 wires electrically coupled through in line zero resistance ammeters divided in ten distinctly controllable groups. This enables the observation of the current evolution as a function of position inside and outside the crevice. A schematic of the conventional half-droplet crevice corrosion attack morphology for a crevice corrosion test with a planar electrode is shown in Figure 1(b). A similar arrangement with a MEA replacing the planar electrode is shown Figure 1(c). The array was assembled from polyimide coated AISI 316 stainless steel wires to ensure electrical insulation from one another. The array was mounted in AISI 316 stainless steel rod (2.54 cm or 1" diameter) to mimic a flush mounted planar electrode and create the surface/volume ratio obtained in planar crevices. The crevice former was made of a polyformaldehyde. The torque applied was transferred through a two component titanium alloy torque applicator (one convex and one concave) that resolved any planarity discrepancy.

The array was ground and polished using SiC paper up to a 1200 grit finish. The crevice former was polished to the same finish and the titanium components were covered with

polytetrafluoroethylene spray to reduce friction. The two components must be able to freely move one against another so that the torque is homogeneously spread out. The experiment consisted of long term anodic potential steps in aerated 0.6 M NaCl solution. The solution was made using reagent grade NaCl and 18.1 M Ω -cm deionized water. The sample was inserted horizontally in a flat cell with an internal coil through which hot water was circulated to maintain the solution temperature at 50°C. The reference electrode was a saturated calomel electrode (SCE) while the counter electrode was a platinum-coated niobium mesh. The crevice former was designed to roughly cover twelve columns of five wires, leaving eight columns open to solution. The AISI 316 mounting rod required one of the ten available groups of the MMA to be potentiostatically controlled. Consequently the last two columns (totaling ten wires outside of the array) were unconnected. A few drops of solution were applied on the array before tightening the crevice former so that solution is present within the crevice from the beginning of the test. The torque used was 2.84 N-m (25 inch-lbs). The creviced array was immersed in the heated solution for two days at open circuit potential to allow the passive film stabilization and solution wicking into the whole crevice. The rod and the uncovered array are kept within the passive range in order to avoid extensive pitting corrosion (outside the crevice) or crevice corrosion (inside the crevice). The value of -25 mV_{SCE} was chosen based on anodic polarization data (in both creviced and uncreviced situations). The creviced array potential was increased by 25 mV increments every 24 hours (equivalent to 3.10⁻⁴ mV.sec⁻¹) to favor crevice corrosion over pitting corrosion, which could occur at faster scan rate. For the first step, the whole array as well as the rod was polarized to -25 mV_{SCE} for one day. The second twenty four hour step saw the increase of the potential for the covered part of the array to 0 mV_{SCE} while the rest of the array (uncovered) and the mounting rod were kept at -25 mV_{SCE}. For the third and final twenty four hour step the

potential of the creviced array was increased to 25 mV_{SCE} while the rest of the groups were held at -25 mV_{SCE}.

The scaling laws describe the effect of geometry on the corrosion behavior of an occluded region. Scaling laws were used to rescale the crevice setup while keeping the corrosion electrochemical properties similar to that of a natural crevice. One of the advantages was to be able to use a commercial alloy available in larger wire sizes and, in the case of arrays, to spread the crevice corrosion over multiple single electrodes so each one of them will have a near homogeneous electrochemical behavior. The initial step was to fit into the model anodic polarization curves of stainless steel AISI 316 in acid solution (1M and 3M HCl) which simulated the crevice electrolyte. Using the software CreviceTM 17-19, the potential and current distribution inside the crevice, as a function of the distance from the crevice mouth, was calculated for various crevice gaps and held potential. The crevice corrosion location x_{crit} is the position where the potential drops below the E_{Flade} . In the present calculations crevice solution composition and pH were assumed to be uniform throughout the crevice. The crevice gap G combined with x_{crit} was used to generate the scaling factor x_{crit}^2/G .

Verification that the coupled MEA yields results similar to planar electrodes was confirmed by comparing anodic polarization data from a creviced flag sample of stainless steel AISI 316L to the anodic polarization of creviced AISI 316 stainless steel array. The potential was swept from -100 mV_{OCP} to 700 mV_{SCE} at 0.1667 mV.sec⁻¹ and held at that potential for one hour. The potential was then swept back to -100mV_{OCP} at the same rate. MEA experiment was performed with the same setup described earlier and the solution was aerated 0.6 M NaCl at 50°C. The creviced planar electrode experiments were performed in 0.6 M NaCl with a sweep rate of 0.1667 mV.sec⁻¹ at ambient temperature.

Results and Discussion

Planar Creviced Electrode vs. Coupled Multi-Electrode Array

The crevice corrosion initiation potential (E_{crit}) and repassivation potential (E_{rep}) were measured for all the wires of the MEA covered by the crevice former during the upward potential sweep test. The average of E_{crit} and E_{rep} of the five rows at a given depth into the crevice was calculated and the standard deviation was determined. These values are shown in Figure 2, as a function of the distance from the crevice mouth along with the E_{crit} and E_{rep} data from planar electrode tests on stainless steel AISI 316L flag samples. To prove that the crevice corrosion behavior of the array is similar to that of the flag sample, the critical potential of the first wire that initiates crevice corrosion on the array should be equivalent to E_{crit} for the creviced planar electrodes. Similarly, the last wire to repassivate should do so at a potential that is close to the repassivation potential of the flag samples. It can be seen in Figure 2 that the first three wire positions displayed E_{crit} and E_{rep} values very close to those found for tests with the planar electrode. Thus, the MEA yields results similar to a conventional electrode.

Scaling Laws

Scaling laws were derived initially from anodic polarization data obtained in acid solution that mimic the acidified pH of crevice solutions. Figure 3(a) shows experimental and fitted anodic polarization curves for AISI 316 stainless steel microelectrodes (250 μm diameter) in 1M HCl and 3M HCl. The potential profile inside the crevice could be calculated at different crevice gaps using CrevicerTM. For a 1M HCl crevice solution, the Flade potential is -200 mV_{SCE} (from Figure 3(a)). The x_{crit} value can be found for the different gap values as the position where the local potential drops below E_{Flade} for a given gap and external potentials of 400 mV_{SCE}, 200 mV_{SCE}, 25 mV_{SCE} and -50 mV_{SCE}. These results are plotted in Figure 3(b) as x_{crit}^2 vs. crevice gap (G) for 1

1 M HCl solution. The horizontal lines represent the physical position of the wires' centers in the array relative to the crevice mouth. For a crevice gap of 1 to 10 μm , a position of severe crevice corrosion would be between the third and the fifth wire and deeper (0.625-1.125 mm from the crevice mouth) for mouth hold potentials of 200 mV_{SCE} and 400 mV_{SCE} . For a mouth potential held at -50 mV_{SCE} , severe crevice corrosion will be observed between the second and the fourth wire and deeper. With a polishing finish of 1200 grit on the array and the crevice former and a 2.84 N-m torque (25 in-lbs), the crevice gap was expected not to exceed 10 μm . Therefore, the scaling law predicts that the dimensions of the crevice should permit the observation of various zones of crevice corrosion as depicted in Figure 1(c). The scaling law also predicts that crevice attack would be the greatest near the mouth and over the zone from 0.5 to 6 mm for a 7 μm crevice gap if the solution inside the crevice is described by electrochemical kinetics similar to those observed in 1 M HCl (Figure 4).

If during the course of crevice corrosion the solution becomes more aggressive (e.g. simulated with 3 M HCl), E_{Flade} will not be observed (see Figure 3(a)) and then crevice attack becomes greatest at the mouth. This is clearly seen on Figure 4 which depicts the model current density as a function of position relative to the crevice mouth for two solutions of different pH with a potential at the mouth of -50 mV_{SCE} .

Long Term Crevice Corrosion of MEA

Figure 5 shows current maps of the controlled coupled multi-electrode array (5 rows by 18 columns). The rectangular solid line represents the region covered by the crevice former (not to scale). Crevice corrosion initiated after five hours at 0 mV_{SCE} on wires B11 and B12 (second and third from the crevice mouth).

Two hours after initiation, crevice corrosion propagated closer to the crevice mouth (column 13) and further inside (column 10) as well as sideways (row D and E). This suggests that an aggressive environment similar to 3 M HCl was present at longer times. The current density will reach high values close to the crevice mouth when the solution acidifies. Over the next three current maps (9 hrs, 11 hrs and 13 hrs) only lateral spreading of crevice attack was observed. All electrodes in columns 10 to 13 have significant crevice attack after 13 hours at 0 mV_{SCE}. The last current map represents the state of the array at the end of the test. The sequence of current maps shows crevice corrosion spreads away from the crevice mouth. Additionally, pitting corrosion is found initiating on six wires outside of the crevice former (on columns 14, 15 and 16). Figure 6 shows the full mounted array as well as a blown up image of the 5*20 wires array after the entire test. The solid gray line represents the position of the crevice mouth. The light gray wires are slightly attacked while the dark gray wires closer to the mouth suffer deeper attack. The dark grey and black wires further from the crevice mouth are unattacked sites and the dark aspect is due to the polished finish that is still present (the same effect can be observed on the bold area of the mounting rod). The corroded wires can be related to the current density map at the end of the experiment, shown in Figure 5. The potential was increased to 25 mV_{SCE} inside the crevice for 1 day after 24 hours at 0 mV_{SCE}. Crevice corrosion spread further inside once the potential increased as observed by the larger number of anodically polarized electrodes in the last map, Figure 5. Figure 6 also shows the effect of crevice corrosion on the stainless steel rod.

The current density versus time behavior of individual wires of row A is shown in Figure 7(a) for a potential of 0 mV_{SCE} under the crevice. It can be seen that the wire A13 is the first to initiate rapidly reaching a maximum current density at which it stabilizes after a peak and a period of noise. At about the same time wires A12 and A11 initiate in a similar fashion, reaching quickly a

maximum current density and stabilizing after a period of noise. The wires A10 and A9 initiate after a delay but follow a similar fashion and reach a maximum current of the order of $10^{-3} \text{ A.cm}^{-2}$. The maximum current was found to decrease when the distance from the crevice mouth increased.

From the currents measured for each position under the crevice, it is possible to derive the depth of attack. Assuming that the depth of attack is homogeneous over the whole surface of the wire and that local cathode currents are small, the total depth of attack at a time t can be given by Equation 1, with EW_{316} being the equivalent weight assuming congruent dissolution of AISI 316 stainless steel, F the Faraday constant, ρ_{316} the density of AISI 316 stainless steel, r the radius of the wire, $I(t)$ the current at a time t , dt the time interval between each measurement and t_0 the initiation time .

$$d(T) = \frac{EW_{316}}{F\rho_{316}\pi r^2} \int_{t=t_0}^{t=T} I(t)dt \quad \text{Equation 1}$$

Figure 7(b) shows a collection of depth profiles derived from the current data using Equation 1. The interval between each curve is fifty minutes. The corrosion rate near the mouth is much higher while it decreases slightly with the distance from the crevice mouth for the rest of the wires as expected from the maximum currents observed. The derived profiles are different than Figure 1(c) in the case of AISI 316 stainless steel, attack quickly becomes greatest at the mouth. However, the maximum depth of attack derived is small compared to the wire diameter. This eliminates the concern of formation of a lead-in-pencil electrode configuration on individual wires. It is notable that growth of crevice corrosion spreads outside the mouth of the crevice former. The depth of attack at this position is quite deep even though the acidified solution

becomes more diluted. It is speculated that this is because of reduced ohmic voltage drop. This will be discussed further in subsequent publications. It should be noted that the experiment duration does not allow the observation of stifling. Future experiments will include Electrochemical Impedance Spectroscopy (EIS) prior to breakdown and stifling.

Conclusion

The MEA has been shown to be useful in the study of crevice corrosion providing spatially and temporally resolved electrochemical measurements on crevice attack. The comparison of critical and repassivation potentials with existing data for planar crevice electrode tests of similar material reveals that the MEA behaves similarly to a plane sample. Scaling laws derived from anodic polarization data offer model x_{crit}^2 vs. G relationships that can be used to adjust the crevice geometry to the dimensions of the MEA. Long step potential tests permit the study of the initiation and growth of crevice corrosion by doing one day potentiostatic tests by small increments (25 mV). Crevice corrosion on AISI 316 stainless steel in 0.6 M NaCl at 50°C was found to initiate at a potential of 0 mV_{SCE} under the crevice. The current for each wire increased sharply to a maximum value and stayed constant afterwards. The further the wire is from the crevice mouth the later it was found to initiate and the lower the maximum current was found to be. The position of the initiation was found to be consistent with the scaling laws predictions. From the current the depth of attack evolution with time can be derived. The depth values obtained (1-50 μm) are realistic with the visual results and the profile is close to that found in the literature. All this confirms the MEA as a sound tool to study crevice corrosion and opens new possibilities by offering spatial current resolution under the crevice.

Acknowledgements:

The support of this work from the Office of Science and Technology and International, Office of Civilian Radioactive Waste Management, U.S. Department of Energy is gratefully acknowledged. The work is carried out as part of the DOE Multi-University Corrosion Cooperative under Cooperative Agreement DE-FC28-04RW12252.

Reference:

1. G78-01: Standard Guide for Crevice Corrosion Testing of Iron-Base and Nickel-Base Stainless Alloys in Seawater and Other Chloride-Containing Aqueous Environments, in *Annual Book of ASTM Standards*, ASTM, (2003).
2. G61-86: Standard Test Method for Conducting Cyclic Potentiodynamic Polarization Measurements for Localized Corrosion Susceptibility of Iron-, Nickel-, or Cobalt-Based Alloys, in *Annual Book of ASTM Standards*, ASTM, (2003).
3. N. D. Budiansky, J. L. Hudson and J. R. Scully, *J. Electrochem. Soc.* , **151**, B233 (2004).
4. N. D. Budiansky, F. Bocher, H. Cong, M. F. Hurley and J. R. Scully, in *Corrosion NACEExpo*, San Diego (2006).
5. F. D. Wall, M. A. Martinez, C. M. Johnson, J. C. Barbour, N. Missert and R. G. Copeland, in *Symposium on Corrosion and Protection of Light Metal Alloys held at 204th Meeting of the Electrochemical Society*, T. E. Society Editor p. p. 1, (2004).
6. W. Zhang, B. Hurley and R. G. Buchheit, *J. Electrochem. Soc.* , B357 (2002).
7. H. W. Pickering, in *CORROSION/ Research Topical Symposium*, J. R. Scully and G. S. Frankel Editors, (2001).
8. J. W. Oldfield and J. W. Sutton, *British Corrosion Journal*, **13**, 13 (1978).
9. S. E. Lott and R. C. Alkire, *J. Electrochem. Soc.* , **136**, 973 (1989).
10. C. S. Brossia and R. G. Kelly, in *Critical Factors in Localized Corrosion II*, P. M. Natishan, R. G. Kelly, G. S. Frankel and R. C. Newman Editors, p. 201, Pennington NJ (1995).

11. B. A. Kehler, G. O. Ilevbare and J. R. Scully, in *CORROSION/Research Topical Symposium*, G. S. Frankel Editor p. 30, (2001).
12. N. J. Laycock, J. Stewart and R. C. Newman, *Corros. Sci.*, **39**, 1791 (1997).
13. M. I. Abdulsalam and H. W. Pickering, *Corros. Sci.*, **41**, 351 (1998).
14. J. R. Kearns, Crevice, in *Corrosion Tests and Standards: Application and Interpretation*, R. Baboian Editor p. 175, ASTM, (1995).
15. R. G. Kelly, Crevice Corrosion, in *ASM Handbook Vol. 13A Corrosion: Fundamentals, Testing, and Protection*, p. 242, ASM, (2003).
16. A. J. Sedriks, Crevice Corrosion, in *Corrosion of Stainless Steel*, 2nd ed., p. 176, Wiley Interscience, (1996).
17. Crevicer website, in <http://www.virginia.edu/cese/research/crevicer.html>, (2002).
18. J. S. Lee, M. L. Reed and R. G. Kelly, *J. Electrochem. Soc.* , **151**, B423 (2004).
19. K. C. Stewart, Intermediate Attack in Crevice Corrosion by Cathodic Focusing, in *Materials Science and Engineering*, University of Virginia, Charlottesville (1999).

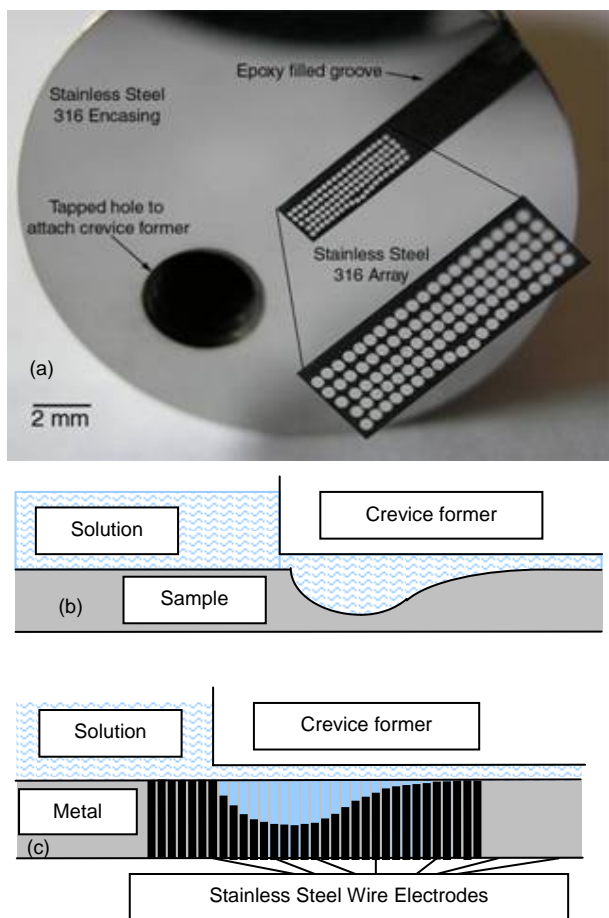


Figure 1. (a) Close packed array of one hundred AISI 316 stainless steel wires (250 μm diameter) in 5*20 arrangement mounted in AISI 316 stainless steel rod. (b) Schematic representation of crevice corrosion attack of a planar sample (c) Schematic representation of multi-electrode array.

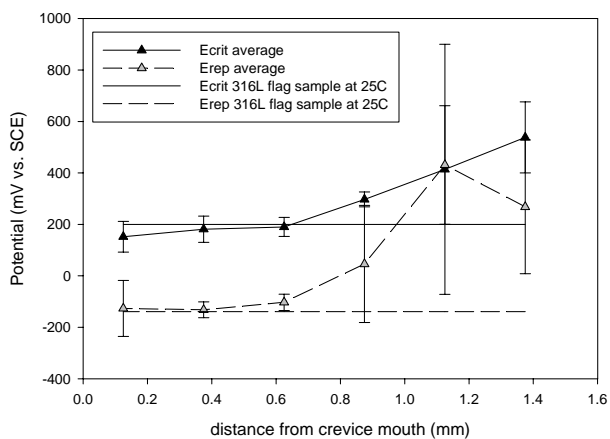


Figure 2. Comparison of the critical potentials (E_{crit} and E_{rep}) obtained from AISI 316L stainless steel creviced planar electrode test and AISI 316 stainless steel MEA test in 0.6 M NaCl at a scan rate of 0.1667 $\text{mV}\cdot\text{sec}^{-1}$ at 50°C (MEA) and 25°C (planar crevice electrode).

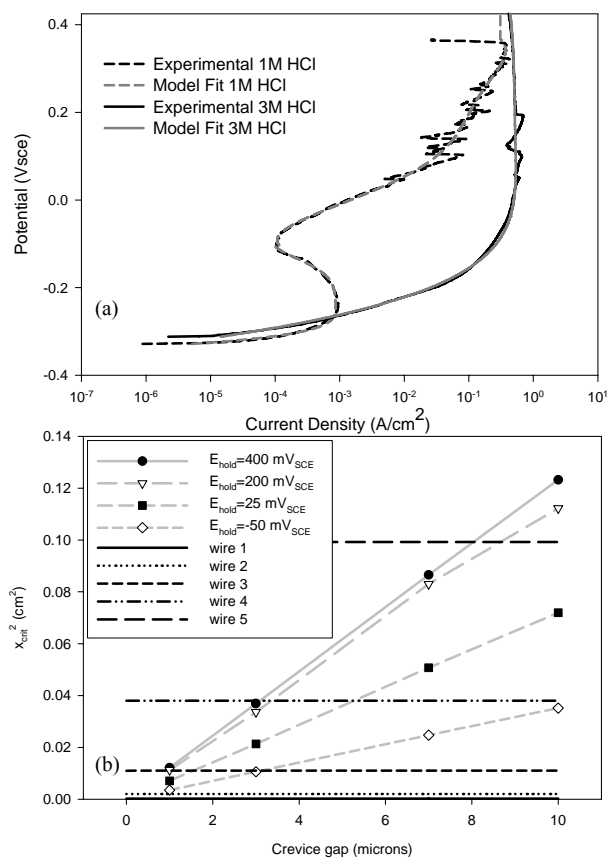


Figure 3. (a) Experimental and model fit of anodic polarization behavior of stainless steel AISI 316 in 1M and 3M HCl

(b) x_{crit}^2 vs. crevice gap scaling laws model based on anodic polarization curves. The horizontal lines represent the position of the wires of an array (wire diam. = 0.25 mm) at different distance from the crevice mouth.

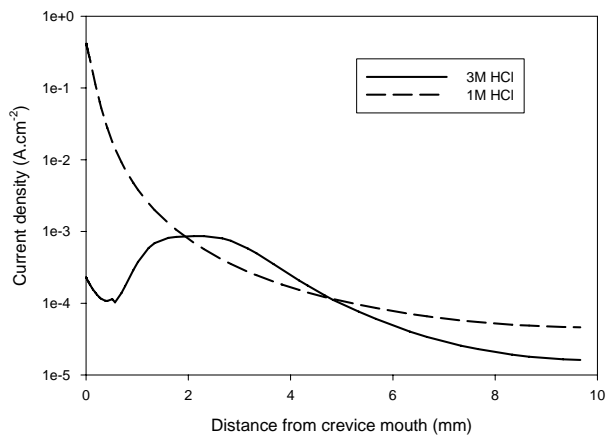


Figure 4. Evolution of the current density with the distance from the crevice mouth for a model crevice solution of 1M HCl and 3M HCl at ambient temperature. The crevice gap is 7 μm and the crevice mouth is held at $-50 \text{ mV}_{\text{SCE}}$.

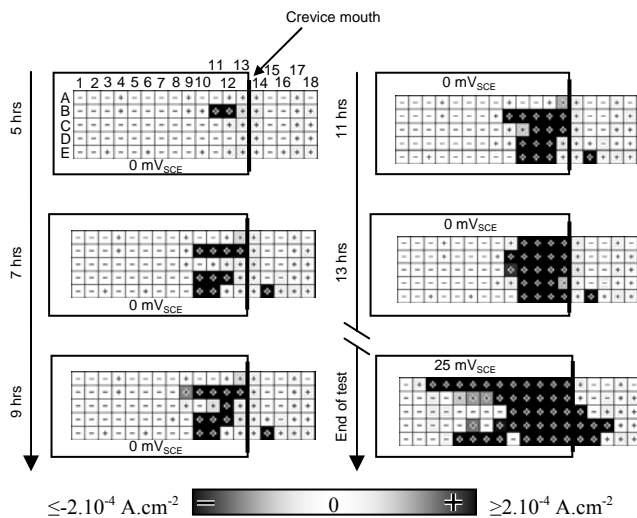


Figure 5. Current density map evolution with time of AISI 316 stainless steel array in 0.6 M NaCl at 50°C. Each square represents a wire with a current density according to the scale. The wires covered with the crevice former are within the rectangles (not to scale). The current density maps show the initiation and propagation of crevice corrosion during the second step at 0 mV_{SCE}. The final map shows the extent of crevice corrosion at the end of the last step.

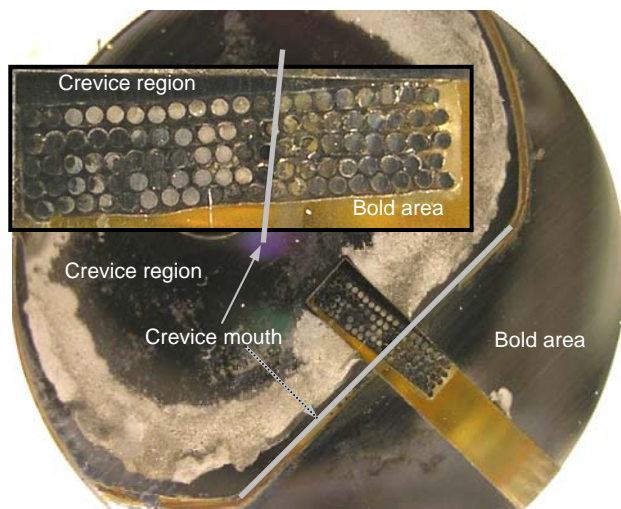


Figure 6. Extent of corrosion on the multi-electrode array (insert) and the full setup after 2 days at OCP, 1 day at -25 mV_{SCE}, 1 day at 0 mV_{SCE} (creviced array) and -25 mV_{SCE} (rest), and 1 day at 25 mV_{SCE} (creviced array) and -25 mV_{SCE} (boldly exposed) in 0.6 M NaCl at 50°C with crevice former applied at a torque of 25 inch-lbs.

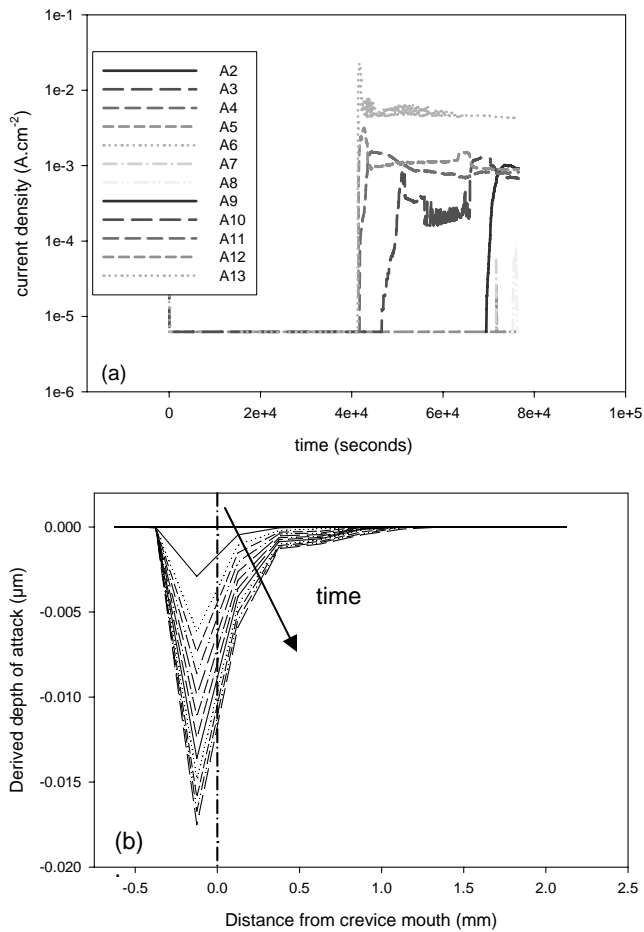


Figure 7. (a) Evolution of current density with times at 0 mV_{SCE} (creviced array) and -25 mV_{SCE} (rest) at 50°C with a torque of 25 inch-lbs at various distance (mm) from the crevice mouth in 0.6 M NaCl.

(b) Attack depth profiles at 50 minute intervals, derived from the current density. The dashed line represents the position of the crevice mouth with the right part being under the crevice.